SEISMIC RESPONSE OF ISOLATED STRUCTURES UNDER SUBDUCTION AND CRUSTAL GROUND MOTIONS: ANALYSIS OF A CASE STUDY STRUCTURE

Fabio FREDDI[1], Juan Carlos DE LA LLERA[2], Fernando GUTIÉRREZ-URZÚA[3], Jorge G. F. CREMPIEN[4], Sahin DEDE[5], José A. GALLARDO[6], Tiziana ROSSETTO[7], Juan Pablo MUÑOZ[8], José CEMBRANO[9], Matías F. CHACÓN[10] & Felipe RIVERA[11]

Abstract: *Seismic isolation aims to uncouple the motion of the structure from the ground shaking and thereby reduce structural forces, accelerations, and deformations of buildings under strong earthquakes. Seismic isolation represents an effective strategy to protect buildings structures, and the related contents from earthquake damage and consequently reduce seismic losses. Nowadays, most of Chile's newly designed hospitals incorporate seismic isolations to minimise structural and non-structural damage and ensure operational continuity even after major earthquakes. Seismicity in Chile is strongly dominated by subduction megathrust events, and most structures, including newly designed hospitals, have been designed and verified by considering the seismic hazard resulting from such earthquakes. However, seismologists have recently highlighted another potential seismic hazard, such as earthquakes originating from the San Ramon Fault (SRF), a crustal fault that lies less than 15 km from the city of Santiago and that was recently declared as potentially active. The present study investigates the seismic performance of a real case study seismically isolated hospital in Santiago, Chile, considering sets of ground motion (GM) records generated by either megathrust earthquakes from the subduction margin or crustal fault mechanism. A 3D finite element model of the case study hospital is developed in OpenSees, including detailed modelling of the seismic isolation system. Sets of recorded subduction GMs, and physics-based synthetic crustal GMs, are selected to perform inelastic response history analyses on the case-study hospital. Local and global Engineering Demand Parameters (EDPs) from the two sets of GMs are compared between them and with code-based capacity limits used during the design. The results show the importance of considering different seismic sources (subduction vs crustal) to better understand/predict the response of isolated structures to GMs.*

Introduction

Subduction megathrust events strongly dominate seismicity in Chile due to the convergence zone between the Nazca and South American plates. Among others, some well-known destructive earthquakes generated by this subduction zone include the 1906 Valparaíso earthquake with moment magnitude M_w = 8.2, the 1960 Valdivia earthquake with M_w = 9.5, and the 2010 Maule (Chile) earthquake with M_w = 8.8 (Ruiz S and Madariaga, 2018). The 1906 Valparaíso earthquake was characterised by a rupture length of about 400 km along the plate boundary, resulting in significant damage throughout central Chile. The destruction was widespread, affecting many cities and towns throughout Central Chile, from Illapel to Talca. The 1960 Valdivia earthquake and tsunami on 22 May 1960 was the most powerful earthquake ever recorded. The epicentre of this megathrust earthquake was near Lumaco, approximately 570 km south of Santiago, with

---

[1] Lecturer, University College London, London, UK, f.freddi@ucl.ac.uk
[2] Professor, Pontificia Universidad Católica de Chile, Santiago, Chile
[3] Catastrophe Risk Analyst, Gallagher Re, London, UK
[4] Assistant Professor, Pontificia Universidad Católica de Chile, Santiago, Chile
[5] PhD Student, University College London, London, UK
[6] PhD Student, Pontificia Universidad Católica de Chile, Santiago, Chile
[7] Professor, University College London, London, UK
[8] Researcher, Research Center for Integrated Disaster Risk Management (CIGIDEN), Santiago, Chile
[9] Professor, Pontificia Universidad Católica de Chile, Santiago, Chile
[10] Researcher, Pontificia Universidad Católica de Chile, Santiago, Chile
[11] PhD Student, University College London, London, UK

Valdivia being the most affected city. The rupture zone for this earthquake was even longer, stretching over 1,000 km along the plate boundary. This event led to many fatalities and monetary losses estimated from US$4.01 billion to $8.021 billion (adjusted to 2022 for inflation). The 2010 Maule (Chile) earthquake and tsunami occurred off the coast of central Chile on 27 February 2010, with intense shaking lasting for about three minutes. It was felt strongly in six Chilean regions (from Valparaíso in the north to Araucanía in the south) that comprise about 80 percent of the country's population. According to official sources, about 9% of the population in the affected regions lost their homes. The losses to the economy of Chile caused by this earthquake are estimated at US$15–30 billion. These and other subduction megathrust events, on one side, have strongly influenced the development of national design standards (INN 1996; INN 2013); on the other side, they highlighted the need for innovative seismic-resilient solutions to ensure the operativity of strategic structures and infrastructures after destructive seismic events (de la Llera *et al.* 2015; de la Llera *et al.* 2017; Simpson *et al.* 2018).

Nowadays, most of Chile's newly designed hospitals incorporate seismic isolations to minimise structural and non-structural damage and ensure operational continuity even after major earthquakes. Over the past 40 years, numerous studies and real-world applications have shown that base isolation is a highly effective method for protecting both new and existing structures against seismic activity. Most recent solutions are based on Lead Rubber Bearings (LRBs) or High Damping Rubber Bearings (HDRBs) in conjunction with Low Friction Sliding Bearings (LFSBs) to achieve long isolation periods. These configurations significantly reduce the forces transferred to the superstructure, resulting in superior performance for base-isolated buildings in both service and ultimate limit states (de la Llera *et al.* 2004; Dall'Asta *et al.* 2022). Most of these seismically isolated structures in Chile have been designed and verified by considering the seismic hazard resulting from subduction megathrust earthquakes.

However, seismologists in Chile have recently highlighted another potential seismic threat close to Santiago, which had previously gone unnoticed. This new hazard originates from the San Ramon Fault (SRF), a crustal fault that extends approximately 35 km in a North-South direction and dips to the East at an angle of about 55° (Diaz *et al.* 2014). Although the SRF was recently identified as being potentially active (Armijo *et al.* 2010), the amount of energy that can release in a single event is still debated; thus, the impact of an earthquake sourced from this fault is uncertain. This is particularly important for structures in Santiago since they have been designed to withstand earthquakes resulting from megathrust subduction events without considering the potential impact of other sources, such as the ones originating from the SRF. Given the proximity to the fault, it is intuitive that such structures could be significantly affected by crustal earthquakes and may not meet the expected seismic performance. To address this knowledge gap, the present study investigates and compares the seismic performance of a case study isolated hospital with HDRBs and LFSBs in Santiago (Figure 1), considering sets of ground motions (GMs) generated by either megathrust subduction or crustal fault mechanisms.
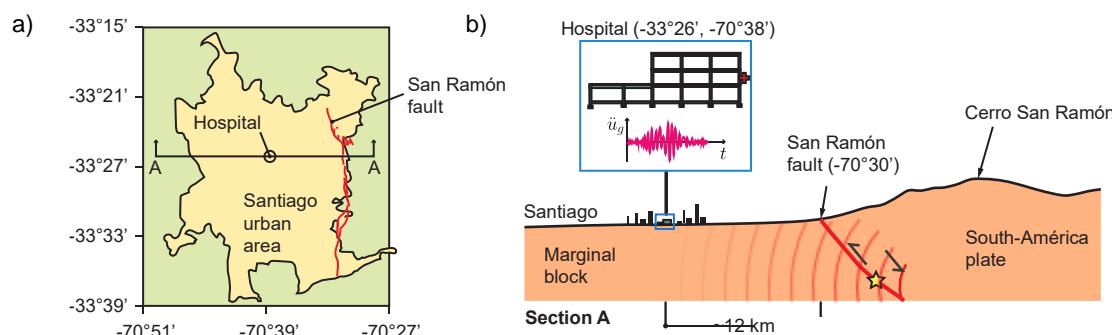

Figure 1. (a) Plan view of the Metropolitan region; and (b) schematic cross-section East-West, including a schematic representation of the San Ramon Fault.

A set of crustal GMs originated by the SRF is generated using the UCSB method (Crempien and Archuleta 2017), which involves simulating a synthetic earthquake source with specified temporal and spatial slip on the fault. For this study, the moment magnitude (M_w), the corner frequency of the moment-rate spectra (f_c), and the average rupture velocity (V_r) are assumed equal to 6.5, 0.14 Hz, and 3.0 km/sec, respectively. These assumptions are considered representative of a realistic

scenario. In addition, a set of 'equivalent' subduction GM records are selected to match the average spectral shape and intensity of the crustal records to allow a fair comparison of the results. A total of 16 records were considered for each of the two sets. A 3D finite element (FE) model of the considered case study hospital is developed in OpenSees (McKenna *et al.* 2000), including detailed modelling of the seismic isolation system. The sets of generated crustal GMs and recorded subduction GMs, are used to perform non-linear time-history analyses on the case-study hospital and investigate its seismic response. Local and global Engineering Demand Parameters (EDPs) are recorded from the two sets of GM records and compared between them and with code-based capacity limits used during the design. The results show the importance of considering different seismic sources (subduction *vs* crustal) to better understand/predict the response of isolated structures to GMs.

Case Studies Structure & Finite Element (FE) Modelling

Case Study Structure

The selected case study hospital is located in downtown Santiago and was subjected to extensive renovation in 2013-2014. The new building comprises two adjacent reinforced concrete (RC) moment-resisting frame structures. The main building, which is the case study of this research work, features a buried substructure with two basements with very stiff retaining shear walls along the perimeter and a superstructure with three stories composed of a regular orthogonal grid of moment-resisting frames spaced at 8.00 m. The isolation level is located at the interface between the sub and superstructure and includes 33 HDRBs and 19 LFSBs. A conventional in-situ floor slab of 180 mm thickness is used for the first basement, while a post-tensioned slab is used for the second basement. The structure is located in seismic Zone 2, and soil type 2 (*i.e.,* very stiff gravel) (INN 2013). Concrete C25 grade with compressive strength f_c = 25 MPa, and steel bars A630-420H grade with yield stress f_y = 420 MPa were used in the design. Figure 2 shows the plan layout and an elevation view of this structure, the location of the different isolator devices, and the characteristics of the HDRBs used in the design. The seismic isolation system was designed using the NCh2745 code design spectrum, corresponding to events with 10% exceedance probability in 50 years (PGA = 0.4g), and the stability of the devices was verified for maximum earthquakes with 10% exceedance probability in 100 years (PGA = 0.48g).
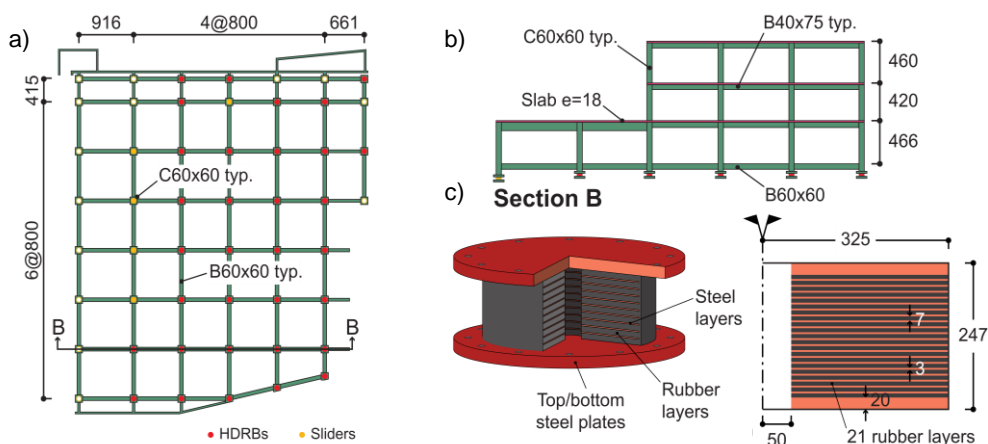

Figure 2. Case-study hospital building: (a) plan view of the isolation system; (b) typical elevation of the isolated structure; and (c) scheme of the HDRBs.

The 33 HDRBs have external and internal diameters of 650 mm and 100 mm, respectively, a height of 247 mm and are characterised by a shear modulus G = 0.392 MPa. The design and the maximum total displacements for the isolators are 239 mm and 249 mm, respectively. Also, the design limits for the short-term axial forces in the HDRBs were assumed as 1.18 MPa in tension corresponding to the cavitation stress (*i.e.,* 3G) (Kumar *et al.* 2015) and 22.56 MPa in compression. At the design displacement, the damping ratio of the rubber was conservatively assumed equal to 9%, while the horizontal stiffness was within the range from 764.92 kN/m to 1029.70 kN/m. The actual value of the damping ratio estimated from experimental tests was approximately 11%. On the other end, the 19 LFSBs have diameters of 350 and 450 mm, and are characterised by a nominal friction coefficient between 5-7% for velocities exceeding 150

mm/s. The maximum axial stresses for the sliders are 15 MPa and 22 MPa, respectively, for long- and short-term loads.

Finite Element (FE) Modelling

Figure 3 shows the 3D FE model of the case study structure that was developed in OpenSees to conduct time-history analyses under the two sets of GM records. The modelling focused only on the superstructure. Modelling of the substructure was neglected as preliminary analyses revealed that, as a consequence of the large stiffness provided by the retaining shear walls, the contribution of the substructure to the dynamic response of the whole building is negligible. Additionally, to reduce the computational efforts required by the analyses, beams and columns in the superstructure (*i.e.*, structural elements above the isolation layer) are assumed to behave elastically and thus modelled as '*elasticBeamColumn*' elements (E_c = 23,500 MPa). This assumption is sustained as these elements were confirmed not to overpass their yielding capacity. A '*rigidDiaphragm*' constraint is included on the nodes at each floor level to represent the diaphragm effect provided by the RC slabs, including the floor above the isolation layer. The gravity load and the seismic mass used for the non-linear time-history analysis correspond to the self-weight plus 25% of the live loads according to the Chilean code (INN 1996) and were uniformly distributed on the slabs at each floor.
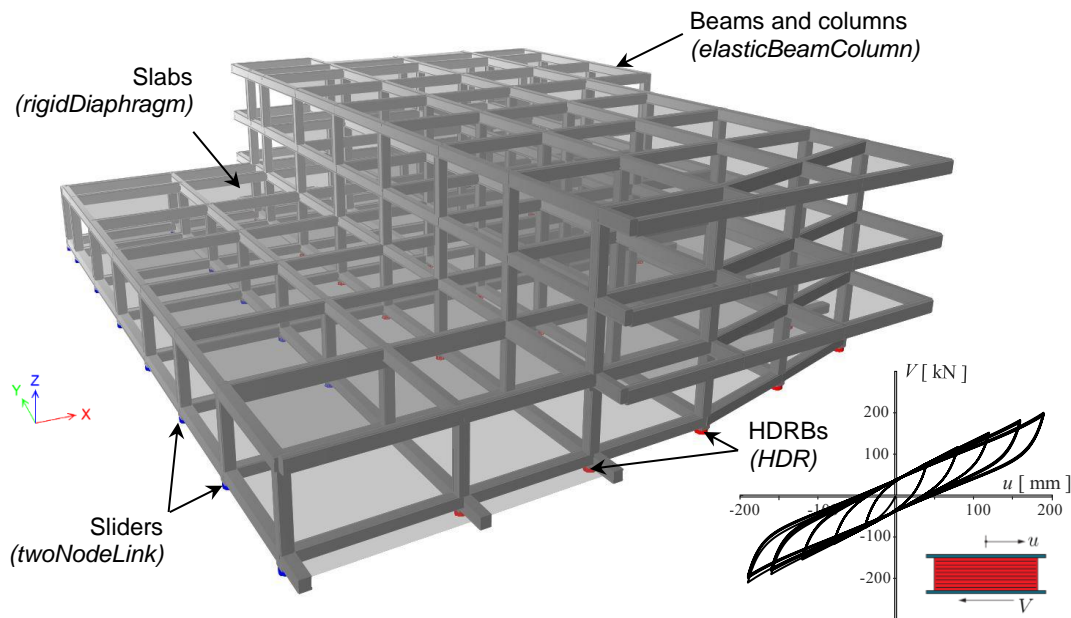

Figure 3. Case-study building: (a) 3D view of the FE model, and (b) shear force-lateral displacement hysteresis of the HDRB model.

The HDRBs were modelled using the 2-node '*HDR*' bearing element in OpenSees, which uses the model proposed by Grant *et al.* (2004) for simulating the shear response, and by Kumar *et al.* (2014) for cavitation under tensile loads. Linear and uncoupled responses were assumed for the axial response and the other three rotational degrees of freedom. Similarly, the LFSBs were modelled by the '*twoNodeLink*' element with the uniaxial '*Elastic*' material in both directions, as it is assumed that their shear stiffness remains largely constant within the drift values considered in this study. A Rayleigh damping model was used for the damping matrix of the superstructure, with a critical damping ratio of 2% for the first two natural vibration modes. This damping only applies to the superstructure as the isolation layer's energy dissipation is explicitly modelled.

Ground Motions (GMs) generation and selection

This section describes the generation of the crustal GMs and the selection of subduction GMs records used for the non-linear time-history analyses of the case-study structure.

Crustal ground motion (GM) records

Crustal GMs originated by the rupture of the SRF have been generated by the UCSB method (Liu *et al.* 2006; Schmedes *et al.* 2013; Crempien and Archuleta 2015; Crempien and Archuleta 2017).

This is done by simulating a synthetic earthquake source with specified temporal and spatial slip on the fault. To propagate waves away from the fault, the procedure relies on the discrete wavenumber technique proposed by Zhu and Rivera (2002), which computes appropriate Green's functions based on a 1D layered velocity structure. The moment magnitude (M_w), the corner frequency of the moment-rate spectra (f_c), and the average rupture velocity (V_r) were assumed equal to 6.5, 0.14 Hz, and 3.0 km/sec, respectively. The corner frequency was forced to have a value consistent with the scaling of this parameter with the magnitude, as proposed by Aki (1967), while the rupture velocity was assumed independent. The spatial characteristics of final slip, rise-time, peak-time, and rupture velocity on the fault were prescribed based on a von Kármán power spectrum correlation structure, with the parameters proposed by Crempien & Archuleta (2015) guiding the correlation structure of the rupture parameters. The fault dimensions were scaled using the relationship proposed by Leonard (2010), which yields a length of 20 km, and a width of 10 km, for the considered M_w 6.5 earthquakes. To account for uncertainties in the GM and by utilising the simulated earthquake source parameters, a total of 16 GM rupture scenarios were produced and computed at the specific location of the case study hospital.

Subduction ground motion (GM) records

Subduction GMs have been selected to be 'equivalent' to the crustal records in terms of horizontal response spectra. The selection procedure is summarised by the following steps:

1. The maximum direction response spectrum (RotD100) is computed for each crustal GM, considering a damping ratio of ξ = 5% and 50 vibrations periods distributed uniformly (in logarithmic scale) between 0.01 s and 5.00 s. The RotD100 was used to select records independently from the directivity effects expected in the crustal GMs, hence making the comparison with the subduction records easier and more meaningful;
2. The mean (in logarithm scale) RotD100 spectrum is computed for the crustal records response spectra at each vibration period;
3. An initial pool of candidate GMs is obtained from the SIBER-RISK seismic database[12], and their RotD100 response spectra are computed;
4. A scaling factor $\alpha^{s,k}$ is computed for each candidate subduction record according to Eq. (1):

$$\alpha^{s,k} = \frac{\sum_{j=1}^{n} S_a^{c,\mu}(T_j)}{\sum_{j=1}^{n} S_a^{s,k}(T_j)} \tag{1}$$

where $S_a^{c,\mu}$ is the mean RotD100 response spectrum of the crustal records, $S_a^{s,k}$ is the RotD100 response spectrum of the k-th subduction candidate GM and T_j's are the periods in the range of interest. Under this condition, only candidate GMs that required a scaling factor between 0.25 and 4.0 were initially considered;

5. One subduction record is selected for each crustal one by computing the sum of squared errors (SSE) between a scaled candidate subduction GM ($\alpha^{s,k} S_a^{s,k}$) and the target crustal GM ($S_a^{c,i}$), in the range of periods of interest (T_j), as shown in the following Eq. (2):

$$SSE_{i,k} = \sum_{j=1}^{n} \left(\ln\left(S_a^{c,i}(T_j) \right) - \ln\left(\alpha^{s,k} S_a^{s,k}(T_j) \right) \right)^2 \tag{2}$$

6. The candidate record with the lowest SSE value is then selected.

By following this approach, the set of selected subduction records closely matches the crustal GMs set in terms of the mean and variance of the RotD100 response spectra. It is worth mentioning that the vertical component is not considered in the selection process but is instead selected as an afterthought and scaled by the same factor used for the horizontal components.

Figure 4 shows the comparison between the response spectra of the set of records for the crustal and subduction GMs in red and black lines, respectively. Bold solid lines represent the mean spectra of the natural logarithm of the accelerations, while the bold dotted lines represent the mean spectra ± one standard deviation. The figure shows how the two sets of records are comparable in terms of horizontal spectral accelerations.

---

[12] https://www.siberrisk.cl/

Dynamic Response and Performance Assessment

Figure 5 shows and reports the natural vibration modes and fundamental periods of the isolated structure. The first two vibration modes are, respectively, in the X- and Y-directions and have long and almost identical lateral vibration periods (*i.e.,* T_1 = 2.849 sec and T_2 = 2.845 sec) due to the presence of the isolation system. The third mode of vibration is torsional and also has a long period but slightly stiffer (*i.e.,* T_3 = 2.719 sec). The higher natural vibration modes are translational (*i.e.,* Mode 4 and 5) and torsional (*i.e.,* Mode 6) and are characterised by similar vibration periods.
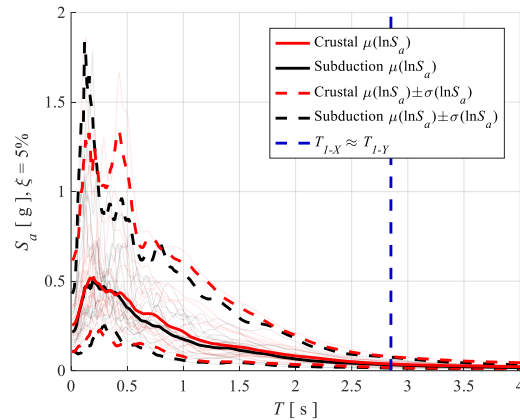

Figure 4. Comparison of the response spectra for the crustal and subduction GMs for horizontal components.

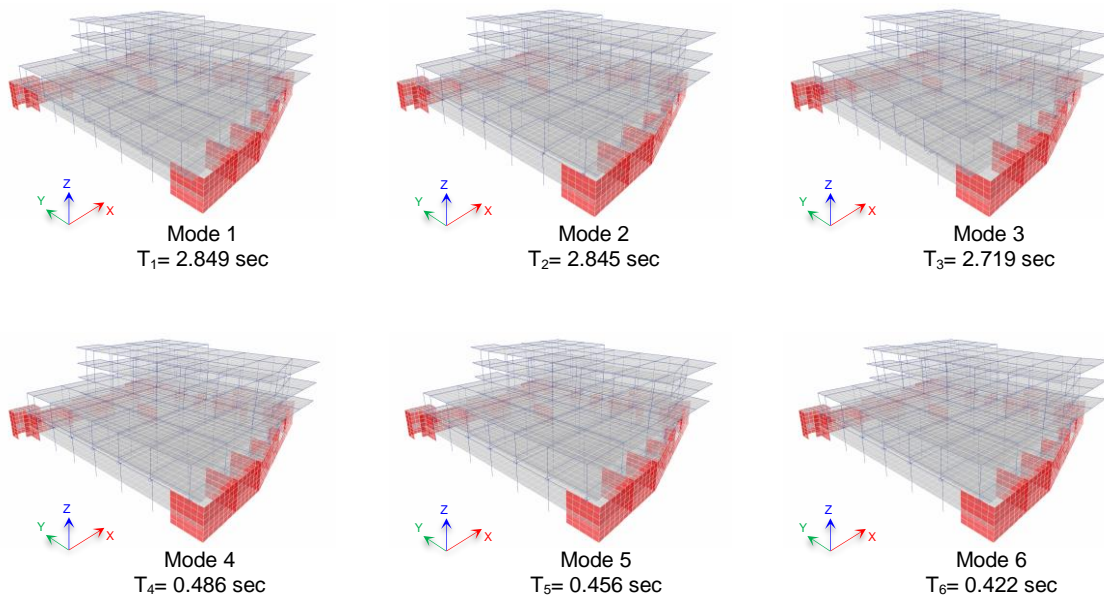|		
Mode 1 T_1= 2.849 sec	Mode 2 T_2= 2.845 sec	Mode 3 T_3= 2.719 sec
Mode 4 T_4= 0.486 sec	Mode 5 T_5= 0.456 sec	Mode 6 T_6= 0.422 sec

Figure 5. Mode-shapes and natural vibration periods.

The time-history analyses are carried out by considering the two sets of 16 GM triplets, as detailed in previous sections. For the crustal GMs, the two horizontal components were applied considering the real orientation of the case-study structure with respect to the seismic sources. Conversely, the subduction GMs records were applied considering the orientation of the records measured at the stations. The following part of the paper describes and compares the response of the structure under the two sets of GMs considering global and local EDPs of interest, *i.e.,* displacements, accelerations, displacements and forces in the HDRBs.

Figure 6 and Figure 7 show the response of the structure, respectively, in terms of displacements and accelerations in X- and Y-directions at the roof and isolation slab for the crustal and subduction GM records. These figures show the orbits for the time-history analyses together with the peak values. The results show minor differences in displacements for the roof and isolation

slab, highlighting the effectiveness of the isolation system in limiting deformations of the superstructure (Figure 6). Some small differences can be observed in terms of accelerations which are slightly amplified due to the response of the superstructure, *i.e.,* slightly higher accelerations at the roof with respect to the isolation slab (Figure 7). The comparison between the results of the two sets of GMs shows that the crustal GMs result in more significant displacement and acceleration demands. Moreover, the response of the structure under this set of records is affected by strong directionality effects. This is a consequence of the strong N-S component of the crustal GMs rather than a property of the building. It is worth reminding the readers that the fundamental periods of the isolated structure are almost identical in X- and Y-directions as a consequence of the isolators. Simulations of the subduction GM records have been carried out also considering them with a 90 degrees rotation, and the results did not show any significant difference in terms of peak values of the considered global and local EDPs. These results are not shown here for the sake of brevity.

Figure 8 shows the local responses in terms of peak horizontal displacements among all isolators and for all records of the two sets of GMs. Consistently with the global responses, it can be observed that the crustal GMs result in larger horizontal displacements. The mean peak horizontal deformation imposed on the isolators (black dotted lines in Figure 8) during the crustal GMs is about 65 mm, contrasting with the approximately 45 mm observed in the subduction GMs. This figure also includes the maximum deformation capacity of the isolators (red dotted lines in Figure 8), showing that, despite the larger deformation demand experienced during crustal GMs, the isolators are still within the design limits. Figure 9 shows the local responses in terms of axial forces of all isolators and for all records of the two sets of GMs. Maximum and minimum demand values for crustal and subduction GMs are reported and compared with demand values deriving from gravity loads only. The figure also shows the mean values for these parameters (magenta and cyan lines in Figure 9), highlighting that crustal GMs generate larger variability of axial forces in the HDRBs compared with subduction GM records. This effect is mainly due to the more significant vertical component of crustal GMs compared with the subduction ones. This figure also includes the design maximum (tension) and minimum (compression) axial force threshold values corresponding to 382 kN and 7309 kN (red dotted lines in Figure 9). In this case, it is observed that the crustal GM records generate demand values overcoming these limits for a few cases.
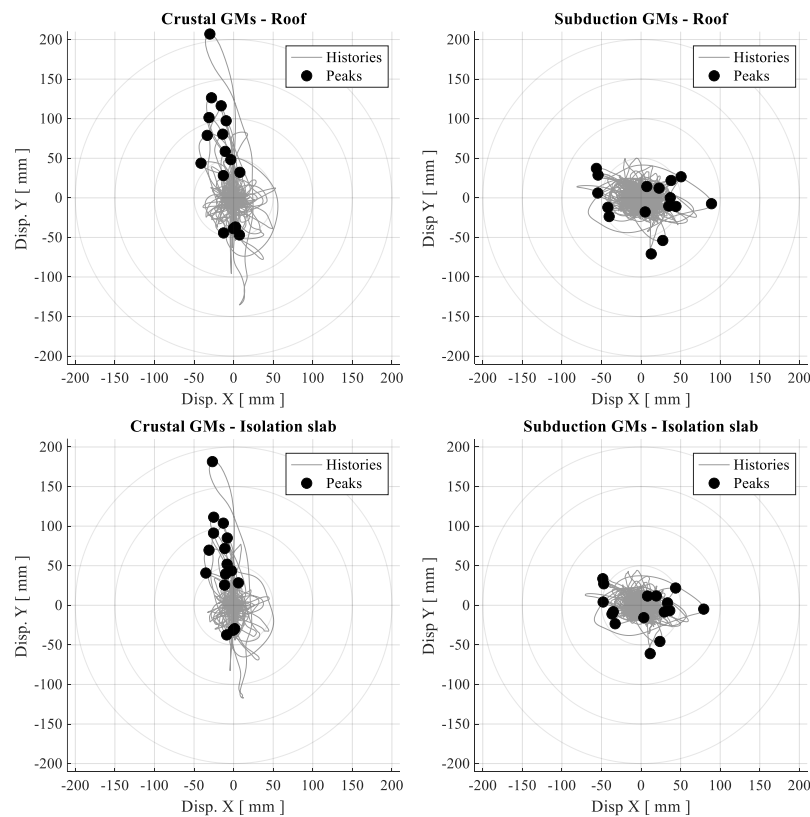

Figure 6. Comparison of displacement orbits for crustal and subduction GM records at the isolation slab and roof.
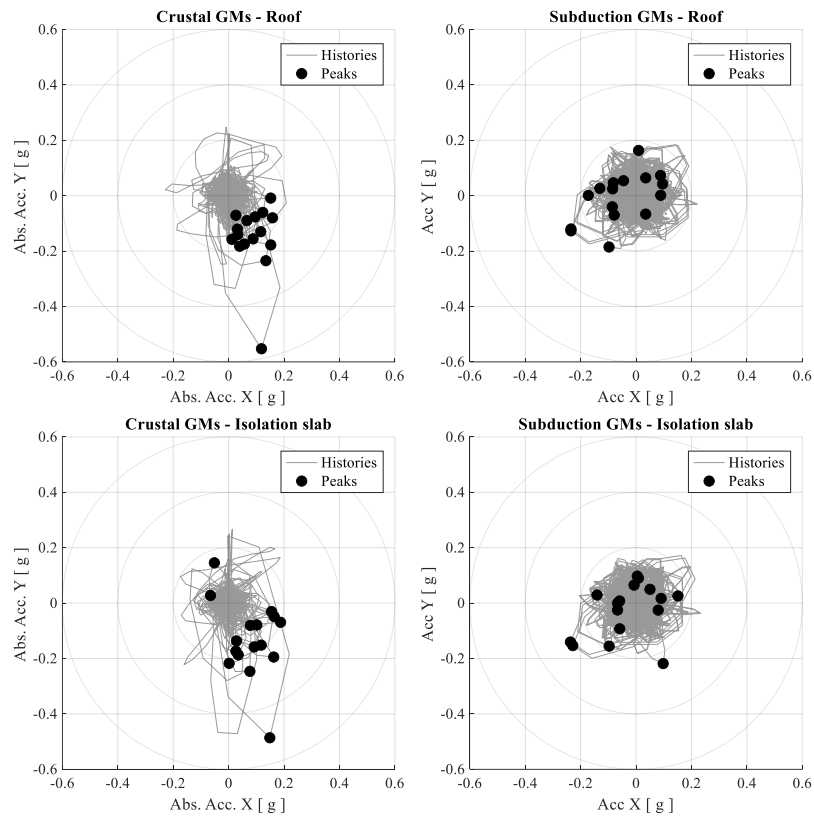
Figure 7. Comparison of absolute acceleration orbits for crustal and subduction GM records at the isolation slab and roof.
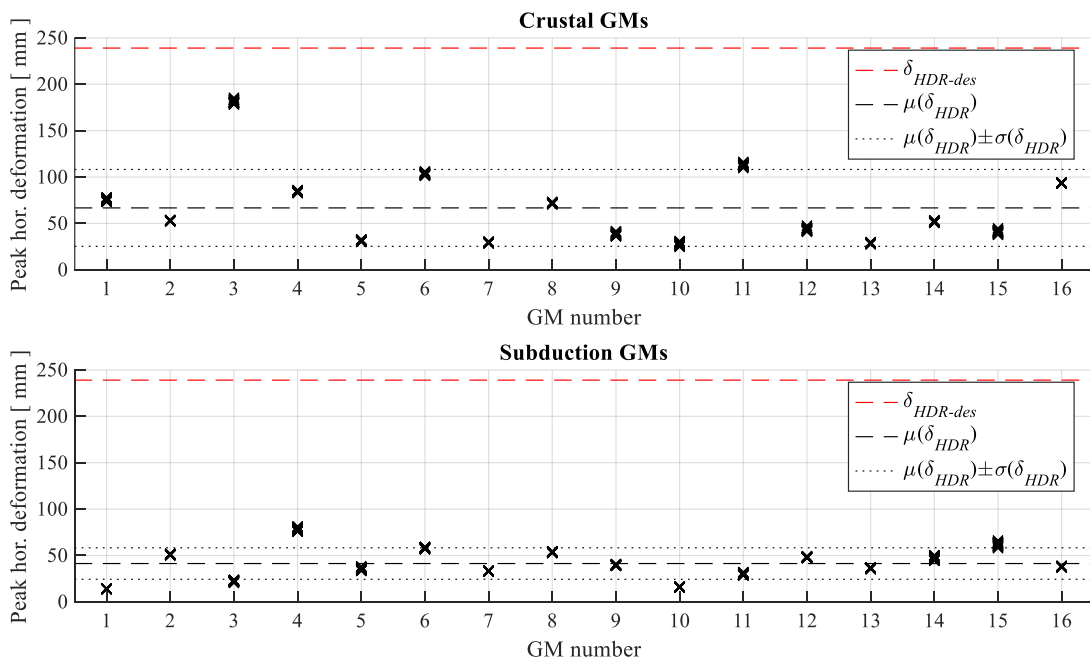

Figure 8. Peak horizontal deformations of HDRB isolators subjected to crustal and subduction GM records.
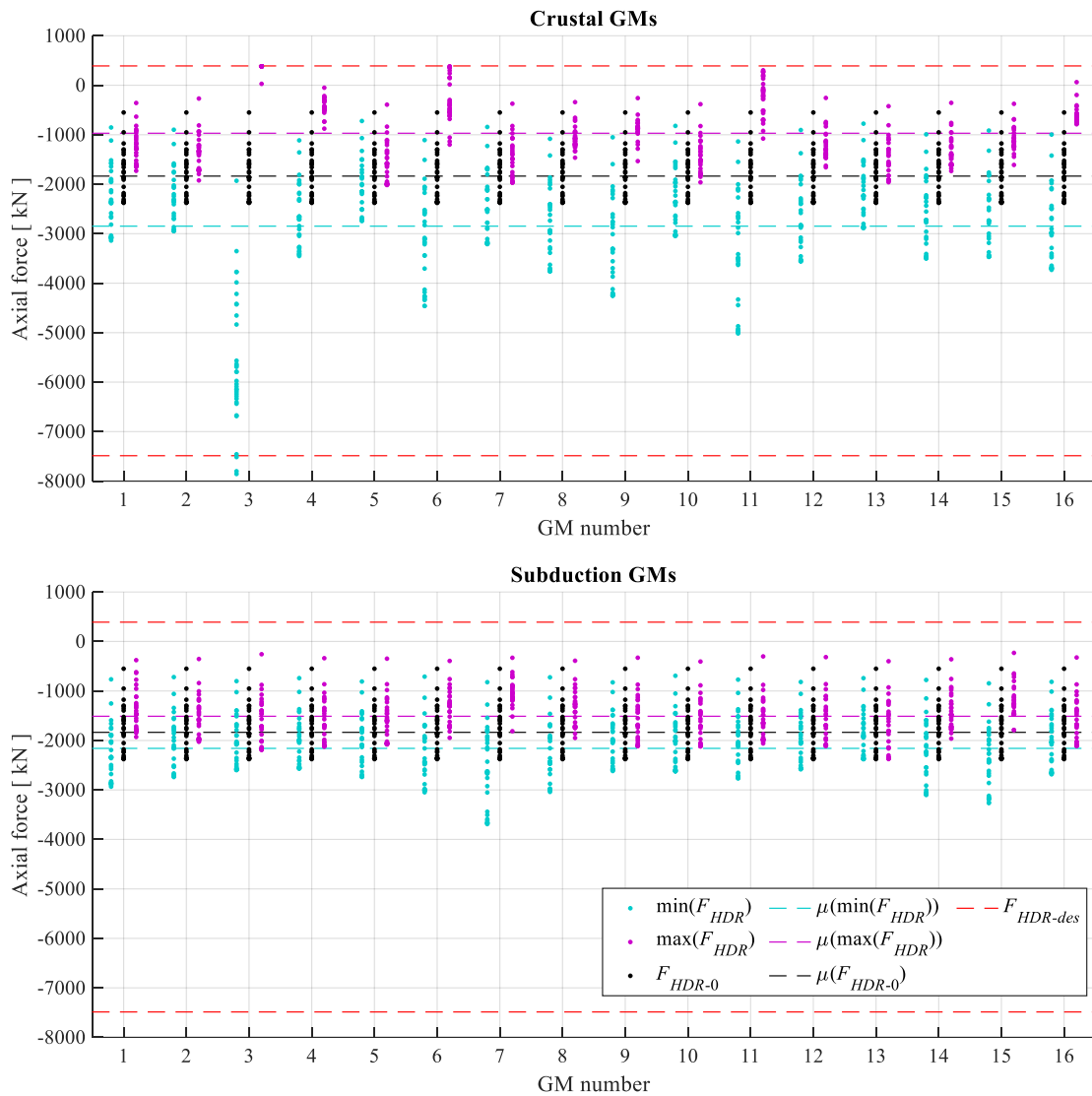
Figure 9. Axial loads imposed on HDRB isolators. Maximum and minimum demand values for crustal and subduction GM records and demand values for gravity loads only.

Conclusions

The present study compares the seismic response of a base-isolated hospital in Santiago, Chile, subjected to crustal and subduction earthquakes. The effectiveness of the seismic isolation system is evaluated by contrasting the response of the structure for each set of ground motion (GM) records and comparing the demands on the isolators to their design limits. The results show that the seismic isolation system is effective in limiting the demands on the superstructure, as the displacements along the height of the building are similar regardless of the GMs type. However, the response of the structure under crustal GMs results in larger displacement and acceleration demands compared to subduction GMs. Despite the larger deformation demand experienced during crustal GMs, the isolators were found within the design limits in all cases. Conversely, it is observed that the axial forces in the HDRBs vary much more with crustal GMs compared to subduction GMs due to the more significant vertical component of crustal GMs. The preliminary results show that, in very few cases, the crustal GM records generate demand values that slightly overcome the design limit states for axial force threshold values.

Acknowledgements

References

Aki, K. (1967). Scaling law of seismic spectrum. Journal of Geophysical Research, 72(4), 1217-1231.

Armijo R, Rauld R, Thiele R, Vargas G, Campos J, Lacassin R and Kausel E (2010), The West Andean Thrust, the San Ramón Fault, and the seismic hazard for Santiago, Chile, *Tectonics*, 29: 1-34.

Crempien J. and Archuleta, R. (2015). UCSB Method for Simulation of Broadband Ground Motion from Kinematic Earthquake Sources. *Seismological Research Letters*, 86, 61–67.

Crempien J. and Archuleta R. (2017). Within-Event and Between-Events Ground Motion Variability from Earthquake Rupture Scenarios. *Pure and Applied Geophysics*, 174, 3451–3465.

Dall'Asta A, Leoni G, Gioiella L, Micozzi F, Ragni L, Morici M, Scozzese F and Zona A (2022). Push-and-release tests of a steel building with hybrid base isolation. *Engineering Structures*, 272: 114971.

de la Llera JC, Lüders C, Leigh P, Sady H (2004). Analysis, testing, and implementation of seismic isolation of buildings in Chile. Earthquake Engineering and Structural Dynamics, 33(5): 543 – 574.

de la Llera JC, Mitrani-Reiser J, Rivera J, Fortuño C, Jünemann R, Poulos A and Vásquez J. (2015). The 2010 Chile earthquake: a five year reflection, In *Proceedings of the 10th Pacific Conference on Earthquake Engineering* (p. 210).

de la Llera JC, Rivera F, Mitrani-Reiser J, Jünemann R, Fortuño C, Ríos M, Hube M, Santa María H and Cienfuegos R (2017). Data collection after the 2010 Maule earthquake in Chile, Bulletin of Earthquake Engineering, 15(2): 555 – 5881

Díaz D., Maksymowicz A., Vargas G., Vera E., Contreras-Reyes E. and Rebolledo S. (2014). Exploring the shallow structure of the San Ramón thrust fault in Santiago, Chile (~ 33.5 S), using active seismic and electric methods. *Solid Earth*, 5(2), pp. 837-849.

Grant D, Fenves G and Whittaker A. (2004). Bidirectional modelling of high-damping rubber bearings. *Journal of Earthquake Engineering*, *8*(spec01), pp.161-185.

INN (2013). NCh2745: Analysis and design of buildings with seismic isolation (In Spanish). *Instituto Nacional de Normalización.*

INN (1996). NCh433: Earthquake resistant design of buildings (In Spanish). *Instituto Nacional de Normalización.*

Kumar M, Whittaker AS and Constantinou M C (2014), An advanced numerical model of elastomeric seismic isolation bearings, *Earthquake Engineering & Structural Dynamics*, 43(13): 1955–1974.

Kumar M, Whittaker AS and Constantinou M C (2015), Experimental investigation of cavitation in elastomeric seismic isolation bearings. *Engineering Structures*, 101: 290–305.

Leonard, M. (2010). Earthquake fault scaling: Self-consistent relating of rupture length, width, average displacement, and moment release. Bulletin of the Seismological Society of America, 100(5A), 1971-1988.

Liu P., Archuleta R., and Hartzell S. (2006). Prediction of Broadband Ground-Motion Time Histories: Hybrid Low / High-Frequency Method with Correlated Random Source Parameters. *Bulletin of the Seismological of America*, 96, 2118–2130.

McKenna F, Fenves GL and Scott MH (2000), *Open system for earthquake engineering simulation (OpenSees)*, University of California, Berkeley.

Ruiz S and Madariaga R (2018), Historical and recent large megathrust earthquakes in Chile. Tectonophysics, 733: 37-56

Schmedes J., Archuleta R., and Lavallee D., (2013). A kinematic rupture model generator incorporating spatial interdependency of earthquake source parameters. *Geophysical Journal International*, 192, 1116–1131.

Simpson B, Kakoty P, Ortega M and Hassan W. (2018). *Resilience reconnaissance for hospitals after the 2010 Maule earthquake*, Technical report, Earthquake Engineering Research Institute (EERI), California.